https://doi.org/10.5194/essd-2021-257
Preprint. Discussion started: 23 August 2021

Open Access Earth System Science Data Discussions

An inventory of supraglacial lakes and channels across the West Antarctic Ice Sheet

Diarmuid Corr[1], Amber Leeson[1,2], Malcolm McMillan[1,3], Ce Zhang[1,2,4], and Thomas Barnes[1]

[1]Centre of Excellence in Environmental Data Science, Lancaster Environment Centre, Lancaster University, Lancaster, LA1 4YQ, U.K.
[2]Data Science Institute, Lancaster University, Lancaster, LA1 4YW, U.K.
[3]UK Centre for Polar Observation and Modelling, Lancaster University, Lancaster LA1 4YW, UK
[4]UK Center for Ecology & Hydrology, Library Avenue, Lancaster, LA1 4AP, U.K.

Correspondence: Diarmuid Corr (d.corr@lancaster.ac.uk)

Abstract. Quantifying the extent and distribution of supraglacial hydrology, i.e. lakes and streams, is important for understanding the mass balance of the Antarctic ice sheet, and its consequent contribution to global sea level rise. The existence of meltwater on the ice surface has the potential to affect ice shelf stability and grounded ice flow, through hydrofracturing and the associated delivery of meltwater to the bed. In this study, we systematically map all observable supraglacial lakes and streams in West Antarctica, by applying a semi-automated Dual-NDWI (Normalised Difference Water Index) approach to >2000 images acquired by the Sentinel-2 and Landsat-8 satellites during January 2017. We use a K-Means clustering method to partition water into lakes and streams, which is important for understanding the dynamics and inter-connectivity of the hydrological system. When compared to a manually-delineated reference dataset on three Antarctic test sites, our approach achieves average values for sensitivity (85.3% and 77.6%), specificity (99.1% and 99.7%) and accuracy (98.7% and 98.3%) for Sentinel-2 and Landsat-8 acquisitions, respectively. In total, we identified 10,478 supraglacial features (10,223 lakes and 255 channels) on the West Antarctic Ice Sheet (WAIS) and Antarctic Peninsula (AP), with a combined area of 119.4 km^2 (114.7 km^2 lakes, 4.7 km^2 channels). 27.3% of feature area was found on grounded ice, 17.8% of feature area comprised lakes which crossed the grounding line, while 54.9% of feature area was found on floating ice shelves. New continental-scale inventories such as these, the first produced for WAIS and AP, are made possible by the recent expansion in satellite data provision. The inventories provide a baseline for future studies and a benchmark to monitor the development of Antarctica's surface hydrology in a warming world, and thus enhance our capability to predict the collapse of ice shelves in the future. The dataset is available at https://doi.org/10.5281/zenodo.5109856 (Corr et al., 2021).

https://doi.org/10.5194/essd-2021-257
Preprint. Discussion started: 23 August 2021

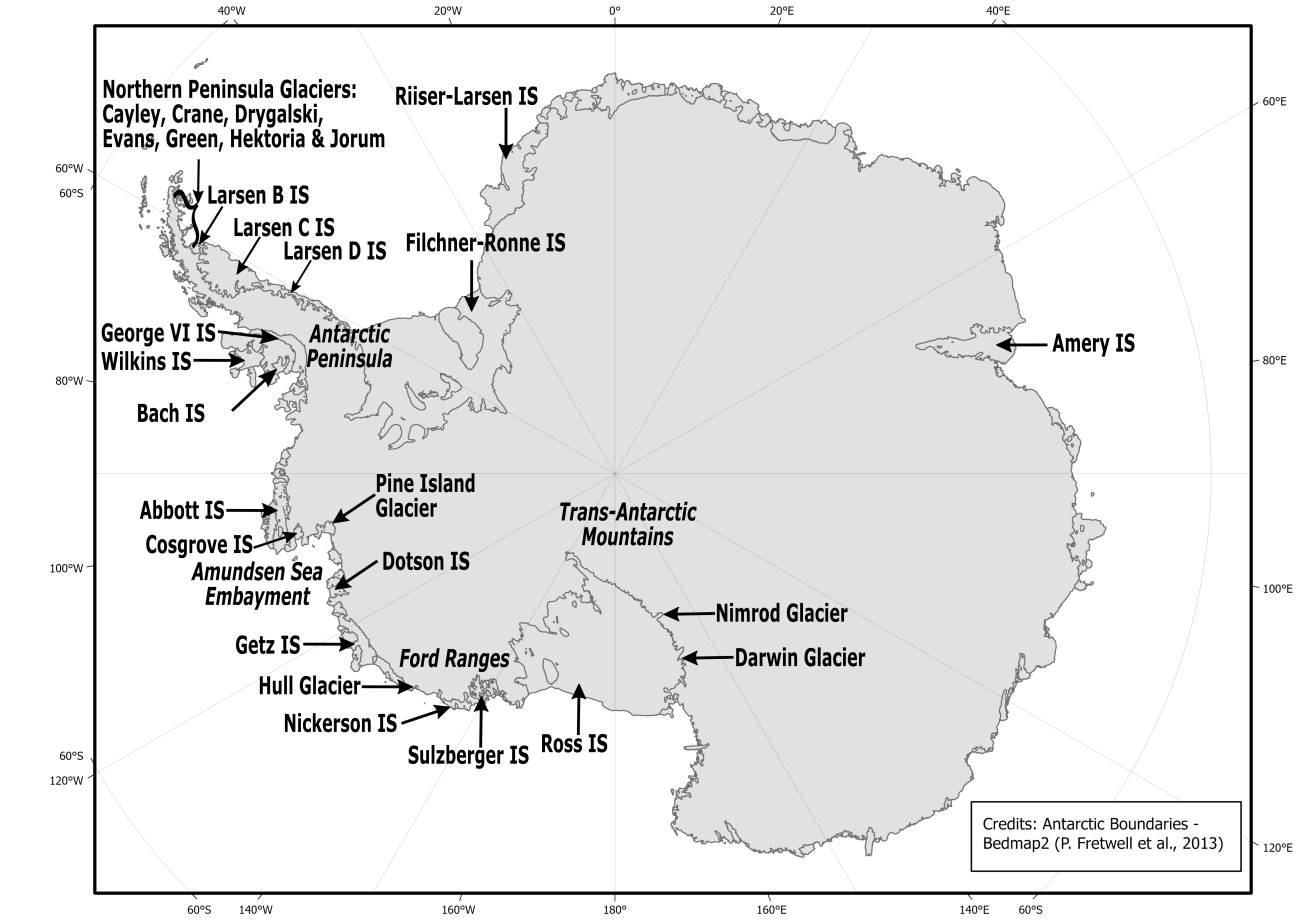

Figure 1. Map of the key locations on the Antarctic Ice Sheet referenced within the paper. Many of the labelled glaciers and ice shelves host supraglacial hydrology features in January 2017. The Antarctic boundaries are according to Bedmap2 (Fretwell et al., 2013).

1 Introduction

The supraglacial hydrological network describes the complex, interconnected system of water movement over the surface of glaciers and ice sheets. The network consists of lakes, channels, moulins and crevasses, and is formed during the summer months when meltwater is generated at the ice surface. The configuration of the supraglacial hydrological network is transient, and determined both by the surface topography and the amount of water in the system at any given time; greater melt, for example, is likely to lead to deeper and more extensive lakes and channels (Tedesco et al., 2012; Luthje et al., 2006; Bell et al., 2018).

https://doi.org/10.5194/essd-2021-257
Preprint. Discussion started: 23 August 2021

Open Access Earth System Science Data Discussions

Supraglacial lakes (SGLs) form when meltwater accumulates in topographic depressions (Bell et al., 2018; Langley et al., 2016). SGLs can drain laterally by overflowing their banks or vertically by hydrofracture, when meltwater flows into fractures on ice surface, increasing the fracture growth (Lai et al., 2020; Scambos et al., 2009). Lateral drainage of meltwater can create new channels in the ice surface connecting lakes to other lakes, to moulins and crevasses or to the ice sheet edge (Bell et al., 2017). Through this interconnected hydrological network, meltwater has been observed to travel more than 120 km, and to be redistributed to regions where no melt has occurred locally (Kingslake et al., 2017).

Several recent studies have shown that, contrary to previous understanding, SGLs are in fact widespread on Antarctica (Kingslake et al., 2017; Langley et al., 2016; Stokes et al., 2019). A continental-scale inventory has been conducted for East Antarctic Ice Sheet (EAIS), but so far not for West Antarctic Ice Sheet (WAIS). Lake coverage in West Antarctica has been assessed through small scale ad hoc studies (Leeson et al., 2020; Banwell et al., 2014; Moussavi et al., 2020). Here, we present a systematic survey of the maximum extent of lakes and large channels on the WAIS and AP during January 2017. Our inventory provides a baseline for monitoring future changes and also serves as a training/forcing dataset for other studies, such as those focused upon methodological development or climate and glaciological modelling. High quality training data are, for example, a vital component of machine learning methodologies, while accurate observations of melt features can act as both boundary conditions and validation for physical models. Knowing the location and characteristics of supraglacial hydrological networks are important on ice sheets because they can alter the location, volume, timing and rate of meltwater drainage (Bell et al., 2018). As such, they provide a possible mechanism through which climate warming and associated increases in surface melt might affect the dynamic stability of Earth's polar ice sheets (Bell et al., 2018; Lenaerts et al., 2016; Trusel et al., 2015).

Vertical lake drainage caused by hydrofracturing occurs when water fills a crevasse in the ice sheet to the point where the water pressure exceeds the fracture strength of the ice (Alley et al., 2018). At this point, the crevasse may propagate through the full ice thickness to the bed, forming a moulin through which the lake drains (Das et al., 2008; McGrath et al., 2012). Rapid lake drainage has been suggested as a mechanism for the breakup of floating ice shelves (Banwell et al., 2019; Scambos et al., 2000), including the disintegration of the Larsen B ice shelf (Figure 1) in 2002 (Banwell et al., 2013; Glasser and Scambos, 2008; Scambos et al., 2003). The breakup of an ice shelf may, in turn, lead to an increase in ice discharge from upstream glaciers (De Angelis and Skvarca, 2003), and an associated increase in their contribution to sea level rise. Following the collapse of the Larsen B ice shelf in 2002, the Hektoria, Green and Evans glaciers accelerated by up to 8 times their original speed (Rignot et al., 2004).

Meltwater which enters cracks, crevasses and moulins on grounded ice drains into the sub- or en- glacial environments (McGrath et al. (2012); van der Veen (2007)). In Greenland, rapid delivery of surface water to the bed has been found to reduce basal friction and temporarily increase ice flow velocities by up to an order of magnitude (Tedesco et al., 2013). It has been hypothesised that mechanisms similar to those observed in Greenland may also occur in East Antarctica (Langley et al., 2016). Indeed, a recent study has shown evidence of five glaciers on the Antarctic Peninsula (Drygalski, Hektoria, Jorum, Crane and Cayley) undergoing near-synchronous speed-up events in March 2017, November 2017 and March 2018 (Tuckett et al., 2019), which suggests that the surface meltwater may have entered into the subglacial hydrological system. The conditions under which drainage occurs and indeed whether lakes can cause hydrofracture, drain rapidly and affect ice shelf

https://doi.org/10.5194/essd-2021-257
Preprint. Discussion started: 23 August 2021

stability on Antarctica, remain unclear. It is possible that supraglacial hydrology may exert a larger effect on Antarctica's future evolution, for example the limit on rise in global temperatures of 1.5°C (UN Paris Agreement's goal is to limit global warming to well below 2°C, preferably to 1.5°C, compared to pre-industrial levels: https://unfccc.int/sites/default/files/english_paris_agreement.pdf) will likely cause the Antarctic Peninsula to experience irreversible, dramatic change to glacial, terrestrial and ocean systems (Siegert et al., 2019). Under this degree of warming (1.5°C), ice shelves will experience continued increase in meltwater production and meltwater will therefore become more extensive (Siegert et al., 2019). The impact of increased meltwater upon ice shelf stability and ice dynamics is not well understood, and therefore mapping the distribution and evolution of the hydrological system from Earth observation has become a key priority of research.

2 Data and methods

Here, we describe the selection and pre-processing of available Sentinel-2 (S2) and Landsat-8 (L8) satellite imagery, the identification of candidate water pixels (using NDWI) and the approach used to mask cloud, rock, slush, blue-ice and shaded pixels. Additionally, the steps involved in post-processing the data and separating supraglacial lakes and channels are outlined. The methodology differs between sensors as L8 provides thermal information (band 10), whereas S2 does not. Furthermore, thresholds on individual bands (or indices) are specific to the spectral properties of each sensor, and therefore require adjustment for each sensor (Moussavi et al., 2020).

2.1 Satellite imagery

In this paper, we use 1682 S2 satellite images to map supraglacial hydrology in West Antarctica. For locations where no S2 data are available, we include 604 L8 images to supplement our dataset. We assess all available scenes with cloud cover below 10%, from 1st to 31st January 2017 on the WAIS. To maximise coverage on the Antarctic Peninsula, which typically experiences more cloudy conditions, we extend the time period to 10th February 2017, and use scenes with cloud cover up to 40%.

S2 data are freely available as ortho-rectified, map-projected images containing Top-of-Atmosphere (TOA) reflectance data from the Copernicus Open Access Hub: https://scihub.copernicus.eu/. S2 bands 2 (blue), 3 (green), 4 (red), and 8 (near infra-red (NIR)) are captured at a resolution of 10 m, the highest spatial resolution acquired by the sensor. In contrast, bands 1 (short-wave infra-red-SWIR Cirrus) and 11 (SWIR) are acquired at coarse resolution of 60 m and 20 m, respectively, and are therefore re-sampled to 10 m using nearest neighbour interpolation for consistency with red, green and blue (RGB) and NIR bands (Williamson et al., 2018). The S2 pixel values represent TOA reflectance units $\times$10,000 and are known as TOA reflectance integers (reflectance$\times 10^4$).

L8 data are freely available from the United States Geological Survey (USGS) Earth Resources Observation Science (EROS) Centre (https://eros.usgs.gov), and are provided as a Level-1 data product consisting of quantized and calibrated scaled Digital Numbers (DN). Prior to use, L8 images are converted to TOA reflectance or brightness temperature values following the method of (Chander et al., 2009). In addition to conversion to TOA reflectance, the blue, green, red and NIR bands of L8 data are pan-sharpened using an Intensity Hue Saturation method (Rahmani et al., 2010). This increases the resolution from

https://doi.org/10.5194/essd-2021-257
Preprint. Discussion started: 23 August 2021


Open Access Earth System Science Data Discussions

the native 30 m to 15 m, for comparability with S2, which has a native resolution of 10 m. The remaining L8 bands used, 6 (SWIR, 30 m) and 10 (thermal infra-red sensor, 100 m) are also re-sampled, using using nearest neighbour interpolation as with the S2 data.

2.1.1 Normalised Difference Water Index (NDWI) thresholding

Multi-spectral satellite imagery is commonly used to detect open water on ice sheet surfaces (Moussavi et al., 2020; Williamson et al., 2018; Miles et al., 2017; Leeson et al., 2020; Stokes et al., 2019; Langley et al., 2016). These methods exploit differences in the spectral signatures of open water and snow/ice/firn at optical frequencies. The Normalised Difference Water Index (NDWI) performs well in identifying supraglacial lakes in Antarctica, using either NIR and green bands, Eq. (1), or blue and red bands, Eq. (2) (Morriss et al., 2013; Moussavi et al., 2016; Xu, 2006; Stokes et al., 2019; Williamson et al., 2017).

$$NDWI_{\mathrm{GNIR}} = \frac{GreenBand - NIRBand}{GreenBand + NIRBand} \tag{1}$$

$$NDWI_{\mathrm{BR}} = \frac{BlueBand - RedBand}{BlueBand + RedBand} \tag{2}$$

Open water features appear as a dark blue colour in optical satellite images due to the rapid attenuation of red light in water relative to blue light. NDWI ratios are, therefore, well suited to map lakes, as they exploit the properties of lakes which make them more easily distinguished from ice at short optical wavelengths (blue wavelengths), and from snow at long optical wavelengths (red wavelengths) (Morriss et al., 2013; Liang et al., 2012; Pope et al., 2016; Yang and Smith, 2013; Sneed and Hamilton, 2007; Box and Ski, 2007; Moussavi et al., 2020). However, identifying supraglacial lake and channel pixels using NDWI alone is insufficient, because slush, rocks, clouds and shadows can be spectrally similar to water (Moussavi et al., 2020). For this reason, additional processing steps are required to identify and mask these features in each image. The processing chain used to map supraglacial lakes and channels in S2 and L8 imagery is shown in Figures 2 and 3.

2.1.2 Cloud, rock masking and elimination of slush, blue-ice and shaded pixels

Thresholds are applied to individual bands, spectral indices and band combinations, such that water pixels can be isolated based on multiple spectral properties. The first step in this process is to remove areas of exposed rock, which are often misclassified as water by the NDWI algorithm (Figures 2 and 3). For S2 images, rock masks are generated by defining a threshold (<0.9) on a Normalised Difference Snow Index (NDSI - Equation 3). The NDSI divides the difference in green and short-wave infra-red (SWIR) by the sum of these bands. To remove snow and cloud from the rock mask, thresholds are applied to blue (<4000 $\mathrm{reflectance} \times 10^4$) and green (<4000 $\mathrm{reflectance} \times 10^4$) bands (Moussavi et al., 2020). Alongside rock, this mask is also used to remove areas of open ocean, which are found adjacent to ice shelves.

$$NDSI = \frac{GreenBand - SWIRBand}{GreenBand + SWIRBand} \tag{3}$$

https://doi.org/10.5194/essd-2021-257
Preprint. Discussion started: 23 August 2021

Open Access Earth System Science Data Discussions

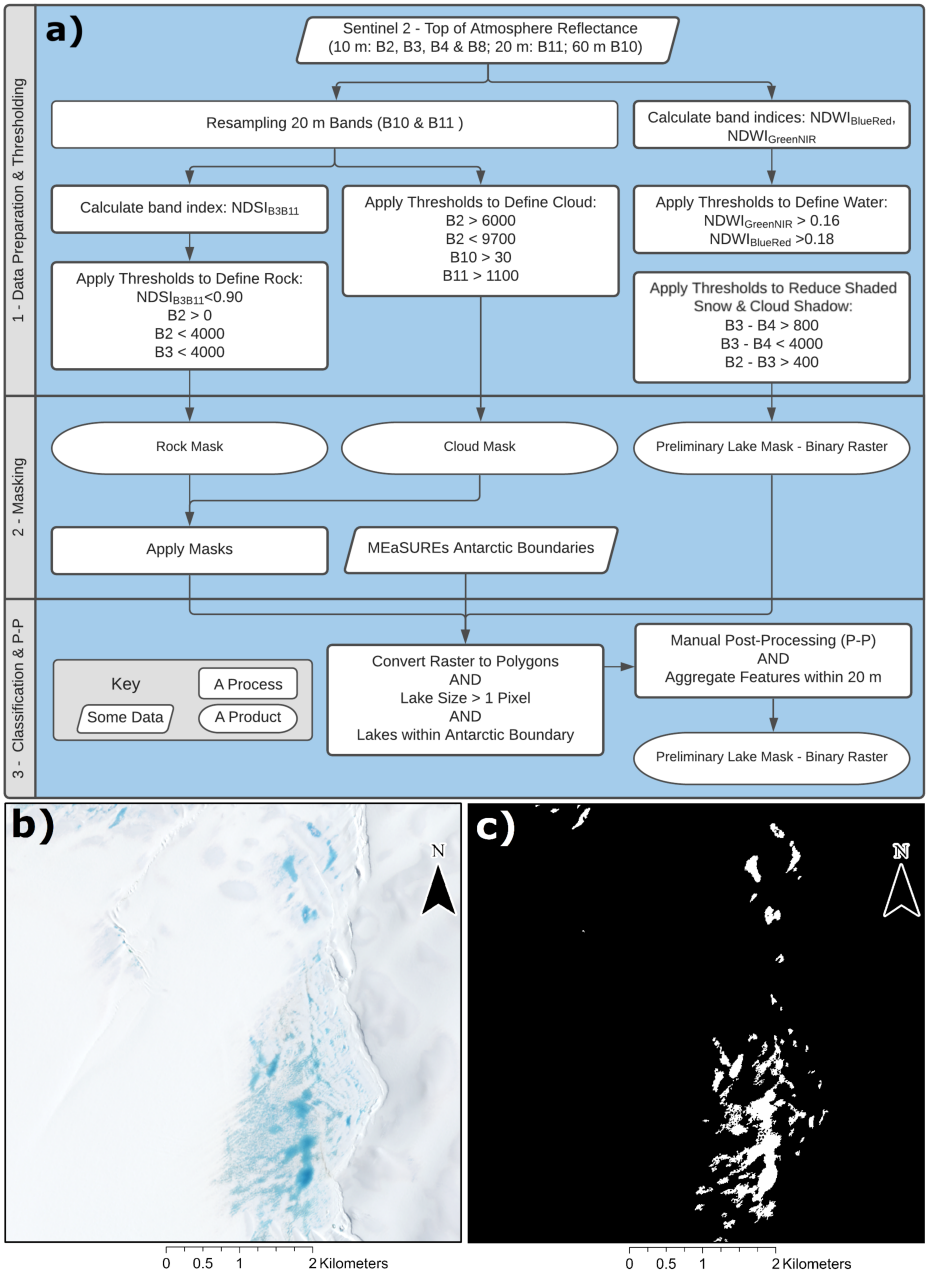

Figure 2. S2 processing chain (a): The input files are the S2 Multi-Spectral Instrument (MSI) products (RGB composite of tile T13CET_20170106 from 06 January 2017 on Pine Island Glacier (b)) and the output is the supraglacial lake and channel binary (surface water - not water) classification (c).

https://doi.org/10.5194/essd-2021-257
Preprint. Discussion started: 23 August 2021

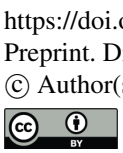

Open Access Earth System Science Data Discussions

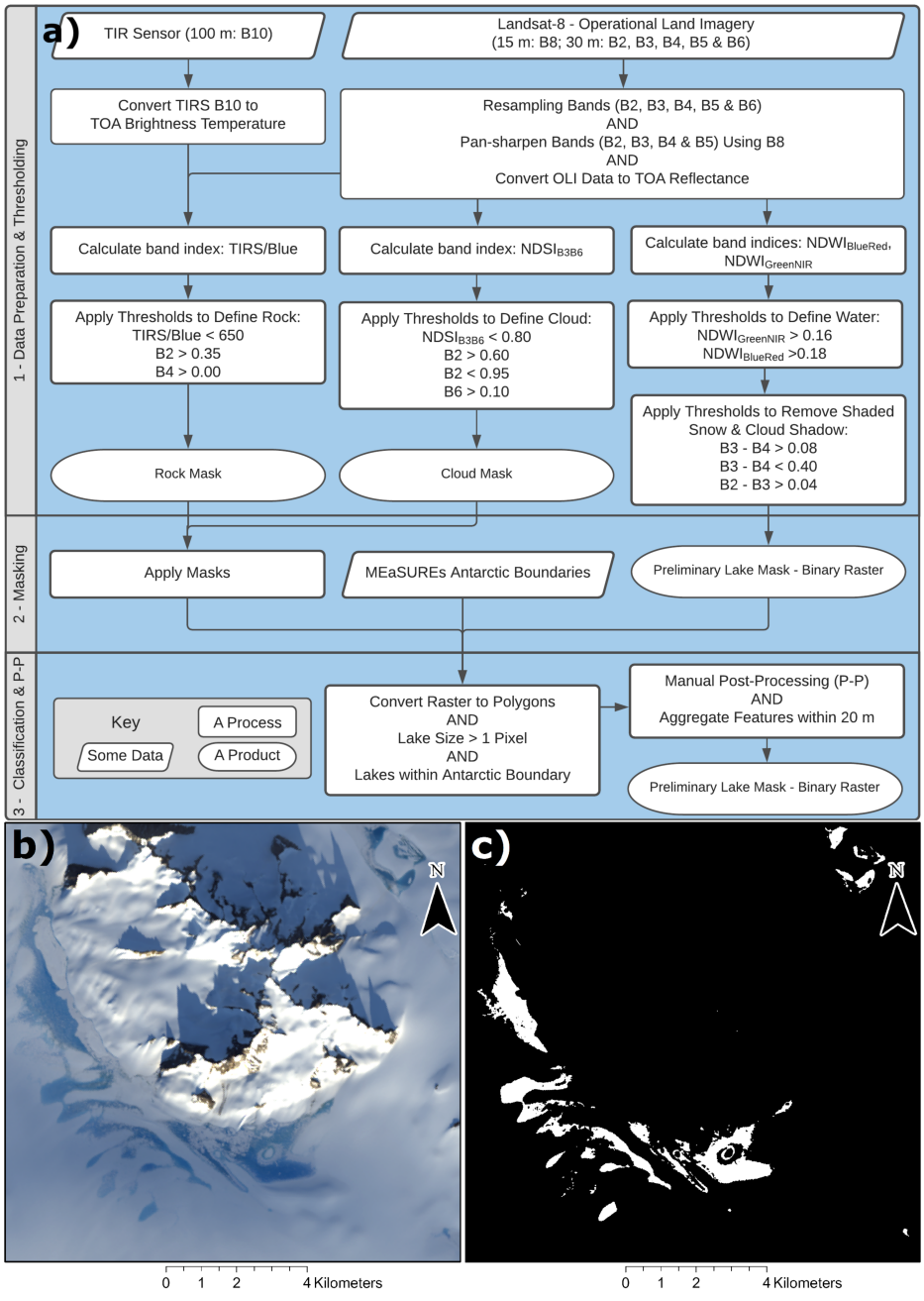

Figure 3. L8 processing chain (a). The input files are the L8 Operational Land Imager (OLI) and Thermal Infrared Sensor (TIRS) products (RGB composite of tile LC08_L1GT_192129_20170118 from 18 January 2017 on Pine Island Glacier (b)) and the output is the final supraglacial lake and channel dataset (c), in raster and vector format.

https://doi.org/10.5194/essd-2021-257
Preprint. Discussion started: 23 August 2021

Open Access Earth System Science Data Discussions

Rock and seawater masking is performed for L8 images by applying a threshold (>650) to the ratio of the blue band and thermal infra-red band (TIRS, Equation 4). To remove snow from the rock mask, a threshold is applied to the blue band (<0.35 reflectance) (Moussavi et al., 2020).

$$\frac{TIRS_1\, BrightnessTemperature}{BlueBand} \tag{4}$$

For S2 imagery, cloud masks are generated by applying thresholds on the blue band of >6000 reflectance $\times 10^4$ and <9700 reflectance $\times 10^4$ and thresholds of >1100 reflectance $\times 10^4$ and >30 reflectance $\times 10^4$ to SWIR and SWIR Cirrus, respectively (Moussavi et al., 2020) (Figure 2). For L8 imagery, a cloud mask is employed using thresholds on the blue (>0.60 reflectance and <0.95 reflectance) and short-wave infra-red (SWIR) bands (>0.10 reflectance) and a threshold of <0.80 on the NDSI equation (Moussavi et al., 2020). For bands that have been resampled to increase spatial resolution (SWIR and SWIR Cirrus for S2, SWIR and LWIR for L8), unwanted edge effects are introduced around the edge of the tiles during the up-sampling process. Thresholds on the red band (>0 reflectance for L8) and blue band (>0 reflectance $\times 10^4$ for S2) are therefore used to remove those edge effects.

Water pixels are extracted using thresholds on two NDWI calculations, Equations 1 and 2. The first step to calculate $NDWI_{GNIR}$ (Equation 1) sets a threshold of 0.16 (for both sensors), above which pixels are considered to have the potential to be water. As stated above, with this threshold alone, the output typically contains slush, blue-ice, shaded rock and cloud shadow pixels. Rock and cloud pixels are removed in their masking processes, respectively. To reduce misclassification of slush and blue-ice pixels, a threshold of 0.18 is further applied to $NDWI_{BR}$ (Moussavi et al., 2020).

To highlight the difference between light attenuation properties in water and shaded snow surfaces, thresholds are applied to combination of blue, green and red bands (Moussavi et al., 2020). Shaded snow and cloud shadows are filtered using 800 (0.08) < green - red < 4000 (0.40) and blue - green > 400 (0.04) for S2 reflectance $\times 10^4$ (and L8 reflectance).

2.1.3 Post-processing

The processing chain outlined thus far generates a binary raster of 'water' and 'not-water' pixels. Groups of water pixels in the raster are subsequently converted into polygons representing discrete lakes or channels. Features smaller than two pixels (200 m^2 in S2 and 450 m^2 in pan-sharpened L8 imagery) are removed from the datasets, as such features are considered to be below the detection limit of the sensors, and more likely to be areas of slush rather than open water (Pope et al., 2016). In addition, all features that are beyond the boundary of Antarctica (i.e. not on grounded ice or floating ice shelves) based on the MEaSUREs coastline of Antarctica (Mouginot and Irvine, 2017) are removed accordingly.

Despite the rock/cloud/shadow masking steps that are applied during image processing, areas of shadow, cloud, rock, crevassing and blue ice can still be misclassified as water, and thus erroneously converted into lake/channel polygons. These 'false positives' are removed manually, with reference to their appearance in a true colour (rgb) composite image during post-processing. ∼50% of images required such post-processing step, mainly due to the presence of misclassified rock and/or shadow. Up to ∼39% (6708) of all 17186 polygons (∼42% of area) delineated automatically are found to be false positives

https://doi.org/10.5194/essd-2021-257
Preprint. Discussion started: 23 August 2021


Open Access Earth System Science Data Discussions

upon manual inspection and subsequently deleted. In total, 10,478 supraglacial features are identified in this study. The majority of all false positives are linked to shaded rock, with either rock in shadow or snow cast into shadow by rock. A few densely populated crevassed regions contribute to ∼20% of misclassified features, but due to their small size (<10 pixels), this represents a much smaller percentage of the total misclassified area.

Although no dedicated checks are carried out to assess the number of false negatives, during the visual inspection for false positives, no large features (>50 pixels) were found to be excluded. Small features (<5 pixels) may remain uncharted, however their influence on the overall area mapped, and therefore the volume of surface water, is likely to be minimal. Finally, overlapping polygons from each sensor, location and time instance throughout January 2017, are dissolved and polygons within a distance of 20 m are aggregated - to provide a more continuous delineation of hydrological connectivity.

2.1.4 Lake vs channel classification

The increased spatial resolution offered by the current generation of optical satellite sensors, such as S2, makes mapping supraglacial rivers and channels possible. Here, in contrast to previous studies in Antarctica, we distinguish between lakes and channels using a K-Means clustering approach (Arthur and Vassilvitskii, 2007), combining six shape index metrics. The first, a standard area-perimeter ratio (A:P), (Equation 5) divides the total area of a feature (A) by the length of its perimeter (P).

$$A : P = \frac{A}{P} \tag{5}$$

Secondly, we use the iso-perimetric quotient (IPQ), (Li et al., 2013), i.e. the ratio of the area of the feature to the area of a circle whose circumference, C, is equal to the perimeter, is applied. This metric is also known as the Polsby-Popper score, when it is used to quantify the degree of gerrymandering of political districts (Polsby and Popper, 1991).

$$IPQ = \frac{A}{\pi(\frac{C_\mathrm{P}}{2\pi})^2} = \frac{4\pi A}{P^2} \tag{6}$$

Providing spatial analysis of complex geographical features can be characterized by fractal dimension. The Fractal dimension index (*Fractal*) (Chen, 2020), reflects shape complexity across a range of spatial scales. Therefore, it overcomes one of the major limitations of the straight perimeter-area ratio as a measure of shape complexity. Depending on the number of vertices in a polygon, the Fractal dimension index can be a variety of logarithmic ratios (Chen, 2020) (Equation 7).

$$Fractal = \frac{2log(\frac{P}{4})}{log(A)} \tag{7}$$

Another metric is the ratio of the feature area to the area of a minimum bounding circle ($\mathrm{A_{MBC}}$) which is needed to enclose the feature (Equation 8). This ratio is known as the Reock score (Reock, 1961).

$$Reock = \frac{A}{A_\mathrm{MBC}} \tag{8}$$

https://doi.org/10.5194/essd-2021-257
Preprint. Discussion started: 23 August 2021


Open Access Earth System Science Data Discussions

To measure compactness of the feature (i.e. how neatly the area fits within the perimeter, most compact shape is a circle) the Schwartzberg score (Inc, 2010) can be calculated (Equation 9). It is the ratio of the perimeter of the feature to the circumference of a circle, C_A, whose area is equal to the area of the feature.

$$Schwartzberg = \frac{1}{\frac{P}{C_A}} = \frac{C_A}{P} = \frac{2\pi\sqrt{\frac{A}{\pi}}}{P} \tag{9}$$

The final metric, a Width-Length ratio (WL) (Equation 10) is calculated as the ratio of the width (W_{MBR}) to the length (L_{MBR}) of the minimum bounding rectangle, which surrounds the feature. The minimum bounding rectangle is the smallest rectangle (by width) required to enclose the full area of the feature.

$$WL = \frac{W_{MBR}}{L_{MBR}} \tag{10}$$

The shape indices (Equations 5-10) were computed for every polygon in the final dataset. Unsupervised K-Means Clustering (Arthur and Vassilvitskii, 2007) was carried out in 6-dimensional space, using each of the six shape indices through the Multivariate Clustering tool on ArcGIS Pro Version 2.5.2 (https://pro.arcgis.com/en/pro-app/latest/tool-reference/spatial-statistics/multivariate-clustering.htm). K-Means algorithms identify a starting point (seed) from among the supraglacial features, to grow each cluster. The first seed was randomly selected, while subsequent seeds were chosen by directing the selection to seeds farthest in data space from the existing seeds. Small lakes, below 500 m^2 in area, introduced noise to the classification and were labelled as lakes prior to clustering. This resulted in 20 distinct clusters which were manually determined to be feature types, of varying shapes and sizes lakes or channels. Through this method, 10,223 lakes and 255 channels were identified to be present during January 2017 on the WAIS and AP (Figure 4).

2.2 Accuracy assessment

The fidelity of our method is tested by comparing our results with 97, 184 and 105 (119, 135 and 46) manually delineated lakes and channels from S2 (and L8) imagery on test sites crossing the grounding line on Amery, George VI and Bach ice shelves respectively (Figure 1). These ice shelves vary in their glaciological and climatological characteristics, which results in a range of feature geometries and settings that are considered to be representative of the whole of Antarctica. On each of the three regions, we selected test regions which encompass extensive surface hydrological meltwater and host close to 100 individual supraglacial features of varying sizes. This resulted in test regions measuring 210 km^2 (for Amery IS) and 100 km^2 (for GVI IS and Bach IS).

Amery ice shelf (IS), the third largest ice shelf in Antarctica, is situated in East Antarctica. The chosen test site on Amery IS is well suited for automated processing due to clear spectral differences between surface water and ice pixels in the region. However, a small area of blue-ice, which has a similar spectral signature to that of open water, is challenging to differentiate automatically. George VI (GVI), one of the largest ice shelves on AP, constrained between the western side of the AP and

https://doi.org/10.5194/essd-2021-257
Preprint. Discussion started: 23 August 2021

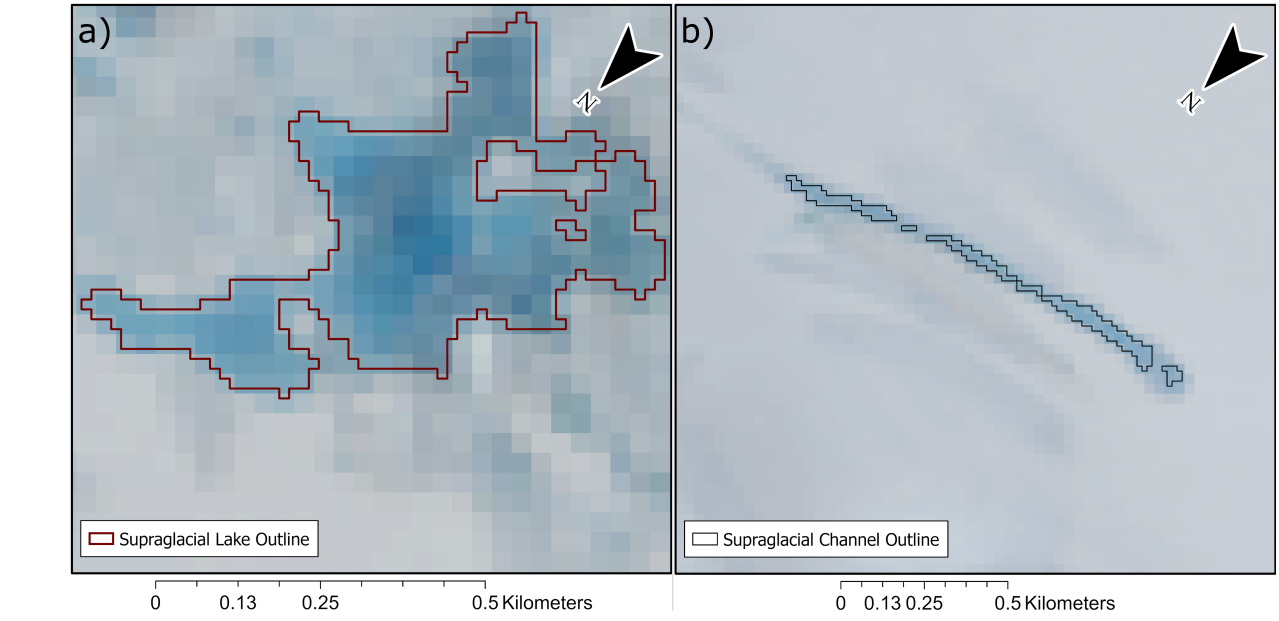

Figure 4. Outlines of supraglacial features over RGB composite of L8 tile LC08_L1GT_022114_20170111 from 11 January 2017. a) SGL covering 0.20 km^2 on Hull Glacier (Figure 1), b) discontinuous supraglacial channel spanning 1.3 km and covering 0.04 km^2 near Hull Glacier.

Table 1. Sensitivity (Sen.), Specificity (Spec.) and Accuracy (Acc.) of the S2 and L8 methodology on each of the test sites: Amery, George VI and Bach Ice Shelves and the mean values across sensors and sites for each.

Test Site	**S2 Sen.**	**L8 Sen.**	**S2 Spec.**	**L8 Spec.**	**S2 Acc.**	**L8 Acc.**	**Mean Sen.**	**Mean Spec.**	**Mean Acc.**
Amery	0.930	0.964	0.979	0.992	0.971	0.987	0.947	0.986	0.979
George VI	0.833	0.614	0.995	0.999	0.985	0.982	0.724	0.997	0.984
Bach	0.797	0.750	0.998	0.999	0.992	0.993	0.774	0.999	0.993
Mean	0.853	0.776	0.991	0.997	0.983	0.987	0.815	0.994	0.985

Alexander Island loses most of its mass to melting rather than calving (Roberts et al., 2008). GVI IS has two ice fronts, one situated around 500 km further north and so experiences different climatic conditions (Cook and Vaughan, 2010). The test site, situated around the middle of the ice shelf, crosses the grounding line of Alexander Island and contains rock and shaded pixels presenting a more difficult task for the methodology. Bach ice shelf is situated on the coast of Alexander Island, to the east of the AP. Although, to date, it has shown relative stability in an area where other ice shelves (particularly Wilkins IS) have undergone major collapse (Humbert and Braun, 2008; Scambos et al., 2009), Bach ice shelf could be the next ice shelf

https://doi.org/10.5194/essd-2021-257
Preprint. Discussion started: 23 August 2021


Open Access Earth System Science Data Discussions

under threat of break-up (Cook and Vaughan, 2010). The test region on the Bach ice shelf offers a contrasting stress regime (unconfined vs confined flow) to that of GVI ice shelf, which in turn has the potential to create different types of lake geometry (Scambos et al., 2000; Cook and Vaughan, 2010).

Lakes and channels in each test area are manually delineated using true colour (RGB) composites of S2 and L8 data. Each area is delineated by three separate 'expert' users (with expertise in remote sensing of supraglacial hydrology). The three manual inventories are combined to form a high fidelity reference dataset of lake and channel features where only pixels that are unanimously assigned as 'water' (i.e. identified as water by all three users) are included. To assess the performance of our method, confusion matrices are calculated which compared manual (Man.) and the final automated (Auto.) datasets (following post processing) on a per pixel basis. From the confusion matrices, sensitivity, specificity and accuracy have been derived (Equations 11, 12 and 13).

The sensitivity, or true positive rate, is the number of True Positive (or Man. Water:Auto. Water in a confusion matrix) predictions divided by the number of manually identified water pixels in the test data. It is a measure of how well surface water pixels are correctly identified.

$$Sensitivity = \frac{Man.Water : Auto.Water}{Total\ Man.Water} \tag{11}$$

The specificity, or true negative rate, is the number of True Negative predictions (or Man.Not Water:Auto. Not Water) divided by the number of of manually identified not-water pixels in the test data. It is a measure of how well all other, non-water, pixels are identified.

$$Specificity = \frac{Man.NotWater : Auto.NotWater}{Total\ Man.NotWater} \tag{12}$$

The accuracy is calculated by dividing the sum of True Positive and True Negative predictions by the total number of pixels. It gives a quantitative assessment for the accuracy of all pixels, both water and not water.

$$Accuracy = \frac{\underset{Manual}{Man.} : \underset{Manual}{Auto.} + \underset{Water}{Man.Not} : \underset{Water}{Auto.Man}}{All\ Pixels} \tag{13}$$

Sensitivity, specificity and accuracy values for each test site and sensor are computed, Tables 1. Across both sensors, sensitivity ranges between 61.4% and 96.4%, specificity between 97.9% and 99.9% and accuracy between 97.1% and 99.3%. On average, S2 yields a higher sensitivity (85.3% versus 77.6%) than L8, while values for specificity and accuracy have higher averaged values for L8 than S2.

The large range in sensitivity is likely due to shallow lakes (deemed so by manual users) being classified as ice by the NDWI threshold, especially on GVI and Bach ice shelves, where there are many shallow lakes. In contrast, the range in specificity (i.e. how well non-water pixels are identified) is smaller, because the analysis was carried out after manual post-processing, and misclassified pixels were already removed. This suggests that, for applications where identifying shallow lakes is important, the

https://doi.org/10.5194/essd-2021-257
Preprint. Discussion started: 23 August 2021

Open Access Earth System Science Data Discussions

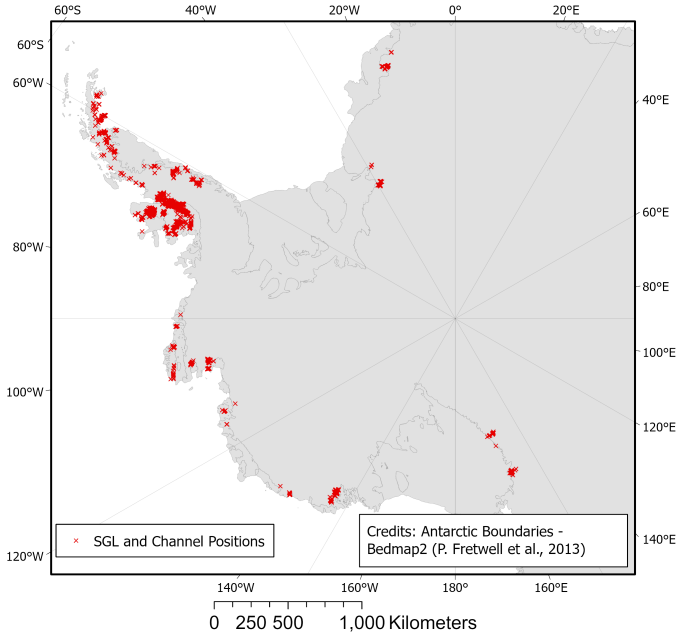

Figure 5. Location of the 10,478 SGLs and channels on the WAIS and AP represented by the red crosses as mapped in S2 and L8 imagery from January and February 2017. Antarctic boundaries are according to Bedmap2 (Fretwell et al., 2013).

sensitivity may be further improved by incorporating additional manual checks for false negatives into the NDWI thresholding approach.

3 Results and discussion

3.1 Distribution of supraglacial lakes and streams in West Antarctica

We used 1682 S2 and 604 L8 scenes to map 10,478 individual supraglacial features in West Antarctica, including the Antarctic Peninsula (Figure 5). The dataset consists of 10,223 SGLs and 255 channels.

SGLs are found in expected regions, on and around the grounding zone of the Antarctic peninsula ice shelves including Larsen C (∼130 lakes), Larsen D (∼250), George VI (∼5,550), Wilkins (∼1450) and Bach (∼950). Lakes are also discovered on grounded ice close to where the remnants of Larsen A (∼10) and B (∼150) ice shelves are located. Sulzberger ice shelf (∼290), Pine Island Glacier (∼360), Riiser-Larsen (∼240) and around the Trans-Antarctic Mountains/Ross ice shelf on Darwin (∼270) and Nimrod (∼90) glaciers, are identified to host SGL activity in this study and others (Kingslake et al., 2017). Studies identifying lakes in the Ford Ranges region (on Hull Glacier (∼45) and Nickerson ice shelf (∼80)) and in Amundsen Sea region (on Dotson (∼35), Abbot (∼125) and Cosgrove (∼45) ice shelves) were published for the first time recently, (Dirscherl et al., 2020; Arthur et al., 2020), and we confirm the occurrence of lakes here during January 2017. 255 supraglacial channels are identified on or around the margin of Larsen C, Larsen D, remnants of Larsen B, GVI, Bach, Wilkins, Riiser-Larsen, Dotson

https://doi.org/10.5194/essd-2021-257
Preprint. Discussion started: 23 August 2021

Open Access Earth System Science Data Discussions

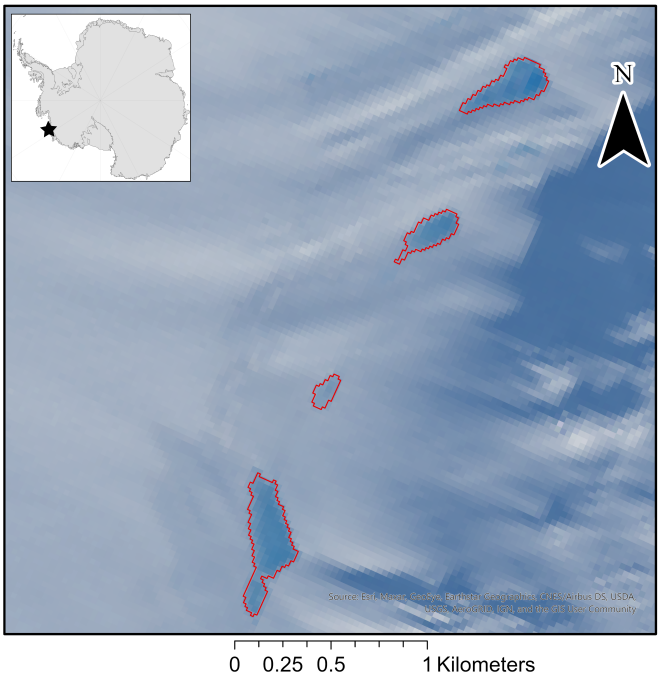

Figure 6. Lakes identified for the first time in the Western Amundsen Sea Sector of West Antarctica, with the largest, southernmost lake of the four crossing the grounding line of the Getz ice shelf. The image is a true colour composite of L8 satellite imagery, Tile LC08_L1GT_166131_20170112 from 12 January 2017. The red outlines are the lake polygons resulting from our NDWI threshold approach. Inset: Getz IS and lake locations in Antarctica.

and Sulzberger ice shelves and near to the Hull and Pine Island Glaciers. Additionally, supraglacial meltwater is identified for the first time on Getz ice shelf, with one lake crossing the grounding line, while a further four border the ice shelf (Figure 6). It has been suggested that increased surface melt on Getz ice shelf will lead to collapse, unless active surface drainage can mitigate the effect of surface loading by exporting water to the ocean (Bell et al., 2018).

The proportion of area covered by meltwater in a localised region (Figure 7) was calculated using the cumulative lake and channel area in a hexagonal bin. Each bin measured 100 m between parallel sides of the hexagon, while any feature within a search radius of 5 km (longest feature: $\sim$4.7 km) contributed to the proportion of the bin in question. The proportions range from 0 (where no lakes are within 5 km of a given bin) to 0.089 km^2 of meltwater area per 1 km^2, with the highest density regions on the Peninsula (George VI, Wilkins and Bach ice shelves), Ford Ranges, Trans-Antarctic mountains and Pine Island Glacier. George VI, which measures $\sim$24,000 km^2 (Cook and Vaughan, 2010), has total meltwater area of 29.4 km^2, and a percentage cover of supraglacial meltwater across the ice shelf of 0.12%. Wilkins (meltwater area: 14.0 km^2, total area: $\sim$11,000 km^2 (Cook and Vaughan, 2010)) and Bach (meltwater area: 13.0 km^2, total area: 4,500 km^2 (Cook and Vaughan, 2010)) ice shelves have maximum percentage cover of 0.13% and 0.29% respectively. Areas with a low proportion of area

https://doi.org/10.5194/essd-2021-257
Preprint. Discussion started: 23 August 2021

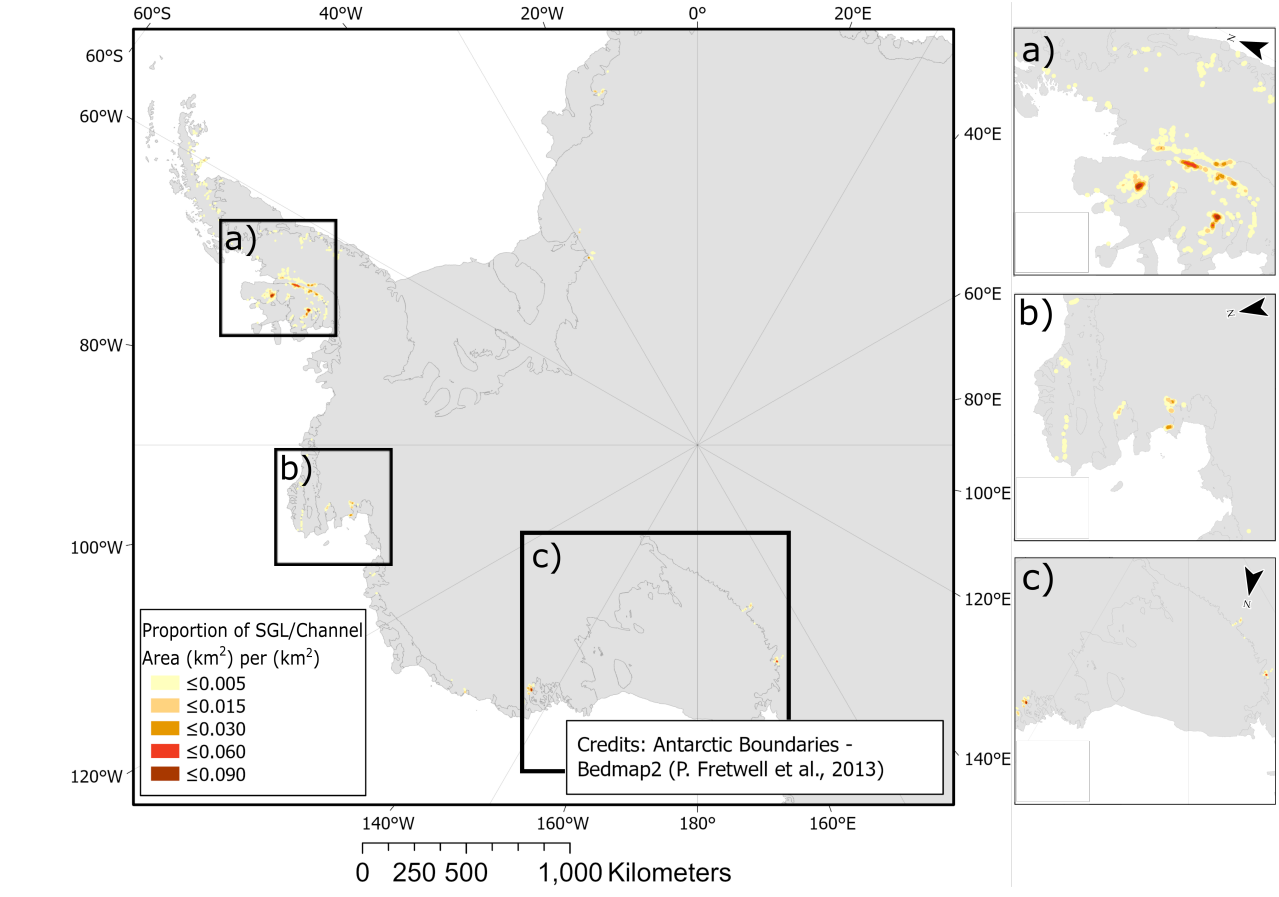

Figure 7. The proportion of lake and channel area covered by meltwater per km^2 in each region on WAIS and AP where surface water is identified. Inset: high cover regions on a) AP (George VI, Wilkins and Bach ice shelves), b) Amundsen Sea region (Pine Island Glacier) and c) Ford Ranges (Sulzberger IS) and Trans-Antarctic mountains (Ross IS, Darwin and Nimrod glaciers). Antarctic boundaries according to Bedmap2 (Fretwell et al., 2013).

covered, hosting just a few lakes include Getz IS, the western margin of the Filchner-Ronne IS, Hull Glacier and on James Ross Island off the coast of the Northern AP.

We have assessed area distribution for SGLs and channels (Figure 8). The total area covered by lakes (114.7 km^2) and channels (4.7 km^2) was found to be 119.4 km^2. The proportion of features on grounded ice (GI), floating ice shelf (IS) and crossing the grounding line (GL) are computed (Figure 9). The distribution of glaciologically important parameters (Figure 10b-f,h) for the 10,478 supraglacial features including, distance to grounding line, exposed bedrock and coastline were calculated. Additionally, ice surface elevation, slope and velocity were observed for each feature and their distribution plotted. Finally, the distribution of meltwater volume was calculated (Figure 10a).

https://doi.org/10.5194/essd-2021-257
Preprint. Discussion started: 23 August 2021

Open Access Earth System Science Data Discussions

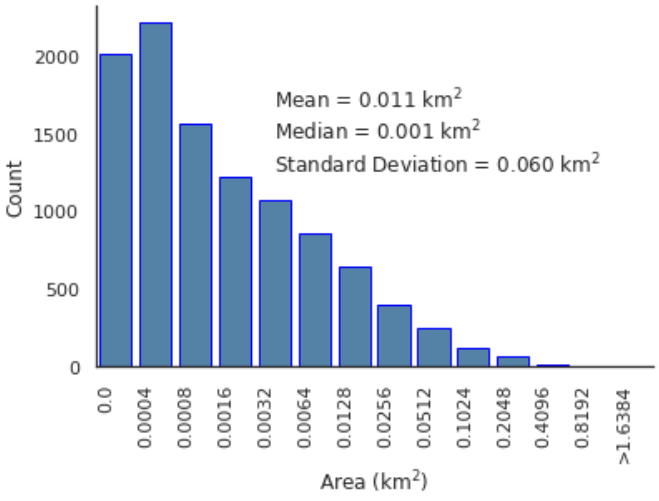

Figure 8. Distribution of SGL and channel area (km^2) on WAIS and AP. Note: bin sizes double from left to right. Values for mean, median and standard deviation for the distribution are included in the figure.

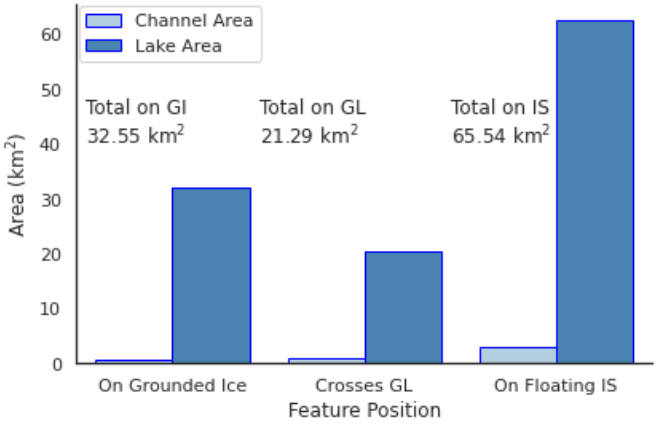

Figure 9. Area split between channels and lakes completely on grounded ice (GI), crossing the grounding line (GL) and completely on floating ice shelves (IS), across the WAIS and AP.

https://doi.org/10.5194/essd-2021-257
Preprint. Discussion started: 23 August 2021


Open Access Earth System Science Data Discussions

The largest lake identified ($\sim$2.9 km^2) intersects the grounding line of the Sulzberger ice shelf, although the majority of lakes and channels are an order of magnitude smaller in size. For example, 8700 (83%) of the features are found to have an area of less than 0.1 km^2 (Figure 8). Lakes make up 96.1% of total feature area and 97.6% of all features (Figure 10g). More than half (54.9%) of the total open water area is found entirely on floating ice, while 27.3% is found on grounded ice entirely (Figure 9). Among the features on grounded ice, the lake found farthest inland of the grounding line is on the Antarctic Peninsula, 47.2 km from George VI ice shelf. In terms of floating ice, the lake found farthest from grounding line is also located on George VI at a distance of 12.6 km. Over half of the open water area (56.4%) is found to be located within 1 km of the grounding line according to Bedmap2 (Fretwell et al., 2013), with 17.8% of total open water area intersecting the grounding line (Figure 10b).

Exposed bedrock has a lower albedo than snow or ice, which can increase the absorption of incoming solar energy, leading to higher rates of melting within the local area. We find that 78.1% of the total feature area (and 80.1% of all features) exists within 10 km of exposed bedrock (Figure 10c). Lakes are also found at substantial distances inland (Figure 10d), including over 504 km away from the closest coastline. Most of the open water however, (64.9% of features and 63.1% of area) is found within 100 km of the coast, according to MEaSUREs data for the coastline of Antarctica (Mouginot and Irvine, 2017; Rignot et al., 2013).

Most features (80.8%, representing 77.5% of the total feature area) are found at low elevations (Figure 10e), i.e. between 0 and 100 m a.s.l, while 87 lakes/channels (or 0.4% of area) are found at elevations greater than 1000 m a.s.l., with two (in the mountain region around 40 km East of GVI ice shelf) as high as 1306 m a.s.l. The majority of lakes/channels (57.9%) occur on surface slopes <1° (Figure 10f). This accounts for 55.7% of the total area.

To estimate the ice flow velocity at the geometric centroid of each feature, we extracted the ice surface velocity from the MEaSUREs InSAR-Based Antarctica Ice Velocity Map (Rignot and Irvine, 2017; Rignot et al., 2011; Mouginot et al., 2012). Ice flow velocities in lake-covered regions ranged from $\sim$0 to >1357 $\mathrm{m/year}$, however 57.8% of the total feature area (and around 47% of the total features) is found on ice flowing slower than 50 $\mathrm{m/year}$ (Figure 10h).

To estimate the volume of water contained within each feature, we use an area-volume (A-V, Equation 14) scaling relationship from literature (Stokes et al., 2019). Based on this relationship, the total volume of meltwater stored in supraglacial lakes and streams is estimated to be 0.085 km^3 across the entire WAIS and AP. Due to proportionality between area and volume, the feature containing the maximum volume of water ($\sim$0.002 km^3) is the lake on the Sulzberger ice shelf, identified as the largest by surface area. 86.9% (>9000 features) of all lakes/channels have volume between 0 km^3 and 0.0001 km^3, while this range accounts for only 17.2% of total area. Conversely, 41.4% of total lake/channel area is represented by just 144 features which have volume greater than 0.0001 km^3.

$$V = 7.16 \times 10^{-4} A \tag{14}$$

3.2 Comparison to supraglacial features in East Antarctica

In combination with a previous study (Stokes et al., 2019), our study provides the first continent-wide assessment of Antarctic supraglacial lakes. We find that, in the austral summer of 2017, the Antarctic ice sheet hosted approximately 76,000 supraglacial

https://doi.org/10.5194/essd-2021-257
Preprint. Discussion started: 23 August 2021

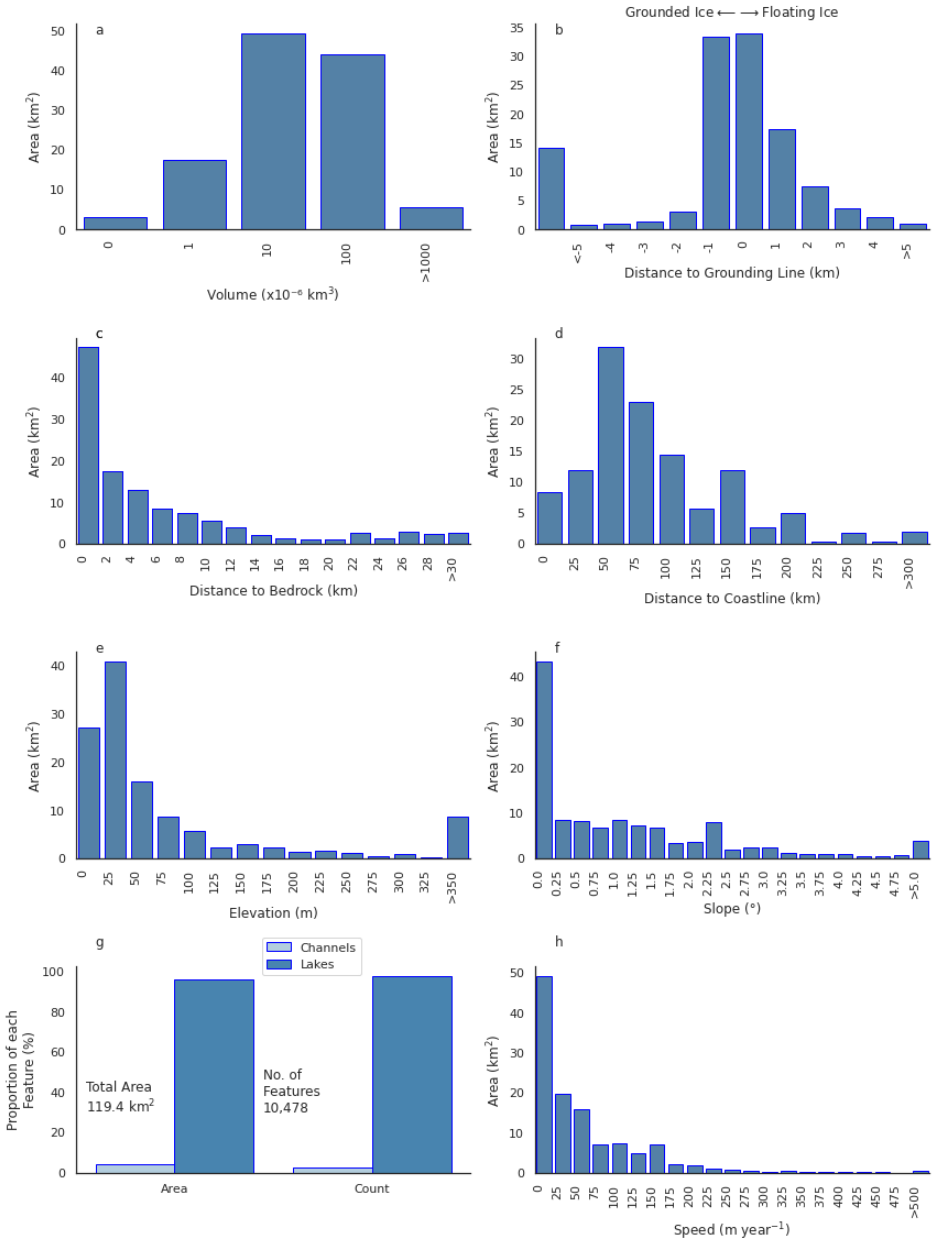

Figure 10. Area distributions of supraglacial lakes and channels on the WAIS and AP according to various glaciological variables. (a) individual feature volumes from the area-volume scaling relationship (Equation 14; (b) distance of each feature to the grounding line (negative values indicate lake/channel positions further inland from the grounding line); (c) distance of each feature to nearest exposed bedrock; (d) distance of each feature to the ice margin/coastline; (e) elevation at the centroid of each feature; (f) the surface slope at the centroid of each feature; (g) area and frequency split between channels and lakes on the WAIS and AP; (h) ice-flow speed for each feature.

https://doi.org/10.5194/essd-2021-257
Preprint. Discussion started: 23 August 2021

features in total, comprising ∼10,500 (119.4 km^2) identified in this study together with ∼65,500 (1383.5 km^2) previously identified in East Antarctica (Figure 11). In total, we estimate 1502.9 km^2 meltwater area and volume totalling 1.08 km^3 (Equation 14) across the entire Antarctic Ice Sheet during the month of January 2017. To ensure complete coverage, we define our WAIS longitudinal boundaries such that they cover all areas not mapped by (Stokes et al., 2019). This results in the Antarctic coastline (measuring ∼35,500 km (Fretwell et al., 2013)) being split approximately equally between WAIS (plus AP) and EAIS. The largest lake recorded within the EAIS dataset (located on Amery IS) measures 71.5 km^2, 25 times larger than the largest WAIS lake which is situated on Sulzberger (IS) (∼2.9 km^2). Amery IS has the highest density of supraglacial lake activity on EAIS with ∼893.3 km^2 total meltwater coverage. Amery IS measures 62,620 km^2 (Foley et al., 2013), meaning the maximum percentage coverage of supraglacial meltwater on the ice shelf is 1.43%, while most densely populated regions in WAIS and AP, George VI, Wilkins and Bach ice shelves are between a factor of five and ten times less (with maximum percentage coverage of 0.12%, 0.13% and 0.29% respectively).

Finally, it is important to note that there are two differences between our approach and that of Stokes et al. (2019), which may result in contrasting classifications. The first is a difference in the methodology used to classify water pixels. Our study attempted to classify both lakes and channels using a dual NDWI approach, while Stokes et al. (2019) focused on SGLs alone. The second source of difference is due to the selection of data used. Where several images are available for specific regions, Stokes et al. (2019) sampled the image closest to the peak melt-season, i.e. mid-January, to provide a snapshot of SGL activity. Consequently, Stokes et al. (2019) report around 6% of the total coastline was not mapped in their study, due largely to the presence of cloud in the scenes. Conversely, our method was designed to quantify the maximum extent of SGL and channels throughout the entire month and to combat the effects of cloud cover, and therefore was based upon a compilation of all available imagery from 1st to 31st January 2017 (and up to 10th February 2017 over the AP).

3.3 Data usage

The dataset described within this study has many potential applications. As NDWI thresholds are the traditional approach to mapping SGL activity on ice sheets, the results of this large-scale study provide a clear picture of the maximum melt extent in January of the 2017 melt-season. Due to the scale of the dataset (across the WAIS) the results provide a baseline for future monitoring of supraglacial hydrology, and could be used to assess regional climate model simulations of surface melting and run-off. Supervised machine learning algorithms require labelled data to train the algorithms. The lake and channel dataset described here will be valuable as training data for pixel-based or object-based approaches in machine learning, such as random forest classification (Dirscherl et al., 2020). The separation of supraglacial features will be beneficial to a machine learning approaches which seeks to distinguish between lake and channel features. Additionally, the dataset produced in this study can be used to assist approaches that utilise other types of satellite data, for example those that exploit Synthetic Aperture Radar imagery but that require an a-priori lake distribution (Miles et al., 2017; Leeson et al., 2020).

Alongside the final map of meltwater extent, the dataset contains meltwater polygons for each sensor (S2 and L8) which forms the final map and are useful for Machine Learning processes. The data's usage for training, validation or independent testing is flexible to the user's choice, providing the data are used alongside imagery from each sensor independently. The

https://doi.org/10.5194/essd-2021-257
Preprint. Discussion started: 23 August 2021

Open Access Earth System Science Data Discussions

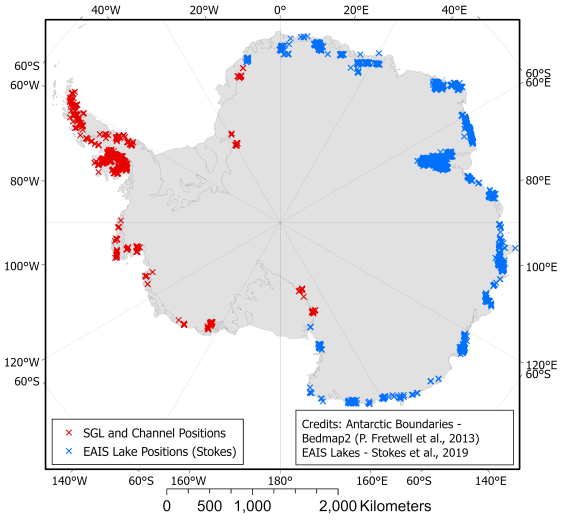

Figure 11. The location of the 10,478 SGLs and channels on the WAIS and AP (red crosses) and 65,459 SGLs (blue crosses; mapped by Stokes et al., 2019) in January and February 2017. Antarctic boundaries are according to Bedmap2 (Fretwell et al., 2013).

dataset can be used entirely for training/testing or if a user prefers, subsetted to provide independent train and test data. The final map of meltwater extent is not to be used for Machine Learning.

4 Conclusions

We have mapped, for the first time, the full extent of supraglacial hydrology on the Antarctic Peninsula and West Antarctic ice shelf during the 2017 melt-season using a Dual-NDWI thresholding approach. We identify 10,223 supraglacial lakes and 255 supraglacial channels (10,478 features in total) which occupy a total area of 119 km^2 (114.7 km^2 lakes, 4.7 km^2 channels). For the first time, supraglacial lakes have been identified on and around the margin of Getz ice shelf, while a significant number of hydrological features are identified on George VI, Wilkins and Bach ice shelves on the Antarctic Peninsula, Sulzberger ice shelf in the Ford Ranges, and Pine Island Glacier in the Amundsen Sea region.

This new inventory provides a baseline Earth System dataset which, in combination with the work of (Stokes et al., 2019), represents the first continent-wide assessment of the supraglacial hydrology of Antarctica. With the operating schedules of the Sentinel-2 and Landsat-8 satellites, optical data are now routinely available at weekly sampling, meaning that it is now possible to expand this study to monitor lake dynamics in near to real time. This will allow for a better understanding of the evolution and dynamics of supraglacial lakes and channels, and how they might change in response to a warming climate. Such approaches would require advanced levels of automation, due to the scale of data required. Importantly, our study provides a high fidelity dataset that can be used to train, calibrate and validate such approaches.

https://doi.org/10.5194/essd-2021-257
Preprint. Discussion started: 23 August 2021

5 Code and data availability

The code used to produce the lake and channel dataset for each sensor (S2 and L8) is written in Python, and can be accessed on Zenodo https://doi.org/10.5281/zenodo.4906097 and GitHub https://github.com/diarmuidcorr/Lake-Channel-Identifier.

The mapped supraglacial lake and channel polygons are available on Zenodo as digital GIS, Geographic Information System, shapefiles (.shp), Keyhole Markup language Zipped (.kmz) and GIS GeoJSON files at https://doi.org/10.5281/zenodo.5109856 (Corr et al., 2021). Datasets exist for the polygons identified on the WAIS and AP. There are three datasets consisting of the final lake and channel polygon maps for both sensors combined (i.e. our final maximum extent map of supraglacial hydrology), plus polygons for each sensor (L8 and S2) individually.

L8 and S2 imagery are freely available at earthexplorer.usgs.gov and scihub.copernicus.eu respectively. Scripts for downloading the data were extracted from GitHub (Hagolle, Olivier, since 2014) and (Hagolle, Olivier, since 2015), however with changes to data structure on both repositories these scripts may no longer be effective. Alternatively, imagery is available to download from Google Cloud Storage (https://cloud.google.com/storage/docs/public-datasets/) using Python scripting (Nunes, Vasco, since 2016).

Author contributions. DC developed the code, carried out the main body of work and drafted this paper. AL, MM and CZ provided supervision and contributed in depth to the science, technical details and structure of this paper. TB conducted data processing, manual post-processing and contributed to methodological development. All authors contributed to the manuscript text.

Financial support. This work was supported by the European Space Agency 4D Antarctica project (contract no. 4000128611/19/I-DT) and a UK Engineering and Physical Sciences Research Council PhD award.

Competing interests. The authors declare that they have no conflict of interest.

Acknowledgements. We would particularly like to thank Laura Melling, for her help in creating manual supraglacial features and Mahsa Moussavi for guidance and support, especially with creating the Dual-NDWI thresholding code. MM acknowledges the support of the UK NERC Centre for Polar Observation and Modelling (grant no. cpom300001) and the Lancaster University-UKCEH Centre of Excellence in Environmental Data Science.

https://doi.org/10.5194/essd-2021-257
Preprint. Discussion started: 23 August 2021

References

Alley, K. E., Scambos, T. A., Miller, J. Z., Long, D. G., and MacFerrin, M.: Quantifying vulnerability of Antarctic ice shelves to hydrofracture using microwave scattering properties, Remote Sensing of Environment, 210, 297–306, https://doi.org/10.1016/j.rse.2018.03.025, <GotoISI>://WOS:000431164300022, type: Journal Article, 2018.

Arthur, D. and Vassilvitskii, S.: k-means++: the advantages of careful seeding, in: Proceedings of the eighteenth annual ACM-SIAM symposium on Discrete algorithms, SODA '07, pp. 1027–1035, Society for Industrial and Applied Mathematics, USA, 2007.

Arthur, J. F., Stokes, C., Jamieson, S. S., Carr, J. R., and Leeson, A. A.: Recent understanding of Antarctic supraglacial lakes using satellite remote sensing, Progress in Physical Geography: Earth and Environment, 44, 837–869, https://doi.org/10.1177/0309133320916114, https://doi.org/10.1177/0309133320916114, publisher: SAGE Publications Ltd, 2020.

Banwell, A. F., MacAyeal, D. R., and Sergienko, O. V.: Breakup of the Larsen B Ice Shelf triggered by chain reaction drainage of supraglacial lakes, Geophysical Research Letters, 40, 5872–5876, https://doi.org/10.1002/2013gl057694, <GotoISI>://WOS:000328210600009, type: Journal Article, 2013.

Banwell, A. F., Caballero, M., Arnold, N. S., Glasser, N. F., Mac Cathles, L., and MacAyeal, D. R.: Supraglacial lakes on the Larsen B ice shelf, Antarctica, and at Paakitsoq, West Greenland: a comparative study, Annals of Glaciology, 55, 1–8, https://doi.org/10.3189/2014AoG66A049, <GotoISI>://WOS:000336010200002, type: Journal Article, 2014.

Banwell, A. F., Willis, I. C., Macdonald, G. J., Goodsell, B., and MacAyeal, D. R.: Direct measurements of ice-shelf flexure caused by surface meltwater ponding and drainage, Nature Communications, 10, https://doi.org/10.1038/s41467-019-08522-5, <GotoISI>://WOS:000458567500010, type: Journal Article, 2019.

Bell, R. E., Chu, W., Kingslake, J., Das, I., Tedesco, M., Tinto, K. J., Zappa, C. J., Frezzotti, M., Boghosian, A., and Lee, W. S.: Antarctic ice shelf potentially stabilized by export of meltwater in surface river, Nature, 544, 344–+, https://doi.org/10.1038/nature22048, <GotoISI>://WOS:000399524400035, type: Journal Article, 2017.

Bell, R. E., Banwell, A. F., Trusel, L. D., and Kingslake, J.: Antarctic surface hydrology and impacts on ice-sheet mass balance, Nature Climate Change, 8, 1044–1052, https://doi.org/10.1038/s41558-018-0326-3, <GotoISI>://WOS:000451919500014, type: Journal Article, 2018.

Box, J. E. and Ski, K.: Remote sounding of Greenland supraglacial melt lakes: implications for subglacial hydraulics, Journal of Glaciology, 53, 257–265, https://doi.org/10.3189/172756507782202883, <GotoISI>://WOS:000248073500010, type: Journal Article, 2007.

Chander, G., Markham, B. L., and Helder, D. L.: Summary of current radiometric calibration coefficients for Landsat MSS, TM, ETM+, and EO-1 ALI sensors, Remote Sensing of Environment, 113, 893–903, https://doi.org/10.1016/j.rse.2009.01.007, <GotoISI>://WOS:000265716000002, type: Journal Article, 2009.

Chen, Y.: Two Sets of Simple Formulae to Estimating Fractal Dimension of Irregular Boundaries, Mathematical Problems in Engineering, 2020, 1–15, https://doi.org/10.1155/2020/7528703, http://arxiv.org/abs/1901.01413, arXiv: 1901.01413, 2020.

Cook, A. J. and Vaughan, D. G.: Overview of areal changes of the ice shelves on the Antarctic Peninsula over the past 50 years, The Cryosphere, 4, 77–98, https://doi.org/10.5194/tc-4-77-2010, https://www.the-cryosphere.net/4/77/2010/, type: Journal Article, 2010.

Corr, D., Leeson, A., McMillan, M., Zhang, C., and Barnes, T.: Supraglacial lakes and channels in West Antarctica and Antarctic Peninsula during January 2017, https://doi.org/10.5281/zenodo.5109856, https://zenodo.org/record/5109856, type: dataset, 2021.

https://doi.org/10.5194/essd-2021-257
Preprint. Discussion started: 23 August 2021

Das, S. B., Joughin, I., Behn, M. D., Howat, I. M., King, M. A., Lizarralde, D., and Bhatia, M. P.: Fracture propagation to the base of the Greenland Ice Sheet during supraglacial lake drainage, Science, 320, 778–781, https://doi.org/10.1126/science.1153360, <GotoISI>://WOS:000255644400035, type: Journal Article, 2008.

De Angelis, H. and Skvarca, P.: Glacier surge after ice shelf collapse, Science, 299, 1560–1562, https://doi.org/10.1126/science.1077987, <GotoISI>://WOS:000181367900033, type: Journal Article, 2003.

Dirscherl, M., Dietz, A. J., Kneisel, C., and Kuenzer, C.: Automated Mapping of Antarctic Supraglacial Lakes Using a Machine Learning Approach, Remote Sensing, 12, 1203, https://doi.org/10.3390/rs12071203, https://www.mdpi.com/2072-4292/12/7/1203, number: 7 Publisher: Multidisciplinary Digital Publishing Institute, 2020.

Foley, K., Ferrigno, J. G., Swithinbank, C., Williams, R. S., and Orndorff, A.: Coastal-Change and Glaciological Map of the Amery Ice Shelf Area, Antarctica: 1961-2004, in: Technical report, USGS Publications Warehouse, Reston, VA, https://doi.org/10.3133/I2600Q, 2013.

Fretwell, P., Pritchard, H. D., Vaughan, D. G., Bamber, J. L., Barrand, N. E., Bell, R., Bianchi, C., Bingham, R. G., Blankenship, D. D., Casassa, G., Catania, G., Callens, D., Conway, H., Cook, A. J., Corr, H. F. J., Damaske, D., Damm, V., Ferraccioli, F., Forsberg, R., Fujita, S., Gim, Y., Gogineni, P., Griggs, J. A., Hindmarsh, R. C. A., Holmlund, P., Holt, J. W., Jacobel, R. W., Jenkins, A., Jokat, W., Jordan, T., King, E. C., Kohler, J., Krabill, W., Riger-Kusk, M., Langley, K. A., Leitchenkov, G., Leuschen, C., Luyendyk, B. P., Matsuoka, K., Mouginot, J., Nitsche, F. O., Nogi, Y., Nost, O. A., Popov, S. V., Rignot, E., Rippin, D. M., Rivera, A., Roberts, J., Ross, N., Siegert, M. J., Smith, A. M., Steinhage, D., Studinger, M., Sun, B., Tinto, B. K., Welch, B. C., Wilson, D., Young, D. A., Xiangbin, C., and Zirizzotti, A.: Bedmap2: improved ice bed, surface and thickness datasets for Antarctica, Cryosphere, 7, 375–393, https://doi.org/10.5194/tc-7-375-2013, <GotoISI>://WOS:000317005200007, type: Journal Article, 2013.

Glasser, N. F. and Scambos, T. A.: A structural glaciological analysis of the 2002 Larsen B ice-shelf collapse, Journal of Glaciology, 54, 3–16, https://doi.org/10.3189/002214308784409017, <GotoISI>://WOS:000254545800001, type: Journal Article, 2008.

Hagolle, Olivier: LANDSAT-Download: Python package for download of Landsat satellite imagery., https://github.com/olivierhagolle/LANDSAT-Download/tree/v1.0.0, since 2014.

Hagolle, Olivier: Sentinel-Download: Python package for download of Sentinel-2 satellite imagery., https://github.com/olivierhagolle/Sentinel-2-download, since 2015.

Humbert, A. and Braun, M.: The Wilkins Ice Shelf, Antarctica: break-up along failure zones, Journal of Glaciology, 54, 943–944, https://doi.org/10.3189/002214308787780012, https://www.cambridge.org/core/journals/journal-of-glaciology/article/wilkins-ice-shelf-antarctica-breakup-along-failure-zones/AD6CDE90DAFB4FC2118EAB4B735C8F2C, publisher: Cambridge University Press, 2008.

Inc, A.: Redrawing the Map on Redistricting: A National Study., Accessedon:21/05/2021http://cdn.azavea.com/com.redistrictingthenation/pdfs/Redistricting_The_Nation_White_Paper_2010.pdf., 2010.

Kingslake, J., Ely, J. C., Das, I., and Bell, R. E.: Widespread movement of meltwater onto and across Antarctic ice shelves, Nature, 544, 349–+, https://doi.org/10.1038/nature22049, <GotoISI>://WOS:000399524400036, type: Journal Article, 2017.

Lai, C.-Y., Kingslake, J., Wearing, M. G., Chen, P.-H. C., Gentine, P., Li, H., Spergel, J. J., and van Wessem, J. M.: Vulnerability of Antarctica's ice shelves to meltwater-driven fracture, Nature, 584, 574–578, https://doi.org/10.1038/s41586-020-2627-8, https://www.nature.com/articles/s41586-020-2627-8, number: 7822 Publisher: Nature Publishing Group, 2020.

Langley, E. S., Leeson, A. A., Stokes, C. R., and Jamieson, S. S. R.: Seasonal evolution of supraglacial lakes on an East Antarctic outlet glacier, Geophysical Research Letters, 43, 8563–8571, https://doi.org/10.1002/2016gl069511, <GotoISI>://WOS:000384443800028, type: Journal Article, 2016.

https://doi.org/10.5194/essd-2021-257
Preprint. Discussion started: 23 August 2021

Leeson, A. A., Forster, E., Rice, A., Gourmelen, N., and Wessem, J. M. v.: Evolution of Supraglacial Lakes on the Larsen B Ice Shelf in the Decades Before it Collapsed, Geophysical Research Letters, 47, e2019GL085 591, https://doi.org/https://doi.org/10.1029/2019GL085591, https://agupubs.onlinelibrary.wiley.com/doi/abs/10.1029/2019GL085591, _eprint: https://agupubs.onlinelibrary.wiley.com/doi/pdf/10.1029/2019GL085591, 2020.

Lenaerts, J. T. M., Vizcaino, M., Fyke, J., van Kampenhout, L., and van den Broeke, M. R.: Present-day and future Antarctic ice sheet climate and surface mass balance in the Community Earth System Model, Climate Dynamics, 47, 1367–1381, https://doi.org/10.1007/s00382-015-2907-4, <GotoISI>://WOS:000382112000002, type: Journal Article, 2016.

Li, W., Goodchild, M. F., and Church, R.: An efficient measure of compactness for two-dimensional shapes and its application in regionalization problems, International Journal of Geographical Information Science, 27, 1227–1250, https://doi.org/10.1080/13658816.2012.752093, https://doi.org/10.1080/13658816.2012.752093, publisher: Taylor & Francis _eprint: https://doi.org/10.1080/13658816.2012.752093, 2013.

Liang, Y.-L., Colgan, W., Lv, Q., Steffen, K., Abdalati, W., Stroeve, J., Gallaher, D., and Bayou, N.: A decadal investigation of supraglacial lakes in West Greenland using a fully automatic detection and tracking algorithm, Remote Sensing of Environment, 123, 127–138, https://doi.org/10.1016/j.rse.2012.03.020, <GotoISI>://WOS:000309496000012, type: Journal Article, 2012.

Luthje, M., Pedersen, L. T., Reeh, N., and Greuell, W.: Modelling the evolution of supraglacial lakes on the West Greenland ice-sheet margin, Journal of Glaciology, 52, 608–618, https://doi.org/10.3189/172756506781828386, <GotoISI>://WOS:000244472100012, type: Journal Article, 2006.

McGrath, D., Steffen, K., Rajaram, H., Scambos, T., Abdalati, W., and Rignot, E.: Basal crevasses on the Larsen C Ice Shelf, Antarctica: Implications for meltwater ponding and hydrofracture, Geophysical Research Letters, 39, https://doi.org/10.1029/2012gl052413, <GotoISI>://WOS:000308308800001, type: Journal Article, 2012.

Miles, K. E., Willis, I. C., Benedek, C. L., Williamson, A. G., and Tedesco, M.: Toward Monitoring Surface and Subsurface Lakes on the Greenland Ice Sheet Using Sentinel-1 SAR and Landsat-8 OLI Imagery, Frontiers in Earth Science, 5, 17, https://doi.org/10.3389/feart.2017.00058, <GotoISI>://WOS:000419394100001, type: Journal Article, 2017.

Morriss, B. F., Hawley, R. L., Chipman, J. W., Andrews, L. C., Catania, G. A., Hoffman, M. J., Luethi, M. P., and Neumann, T. A.: A ten-year record of supraglacial lake evolution and rapid drainage in West Greenland using an automated processing algorithm for multispectral imagery, Cryosphere, 7, 1869–1877, https://doi.org/10.5194/tc-7-1869-2013, <GotoISI>://WOS:000328546300014, type: Journal Article, 2013.

Mouginot, J. and Irvine, U. O. C.: MEaSURES Antarctic Boundaries for IPY 2007-2009 from Satellite Radar, Version 2, https://doi.org/10.5067/AXE4121732AD, https://nsidc.org/data/nsidc-0709/versions/2, type: dataset, 2017.

Mouginot, J., Scheuchl, B., and Rignot, E.: Mapping of Ice Motion in Antarctica Using Synthetic-Aperture Radar Data, Remote Sensing, 4, 2753–2767, https://doi.org/10.3390/rs4092753, http://www.mdpi.com/2072-4292/4/9/2753, 2012.

Moussavi, M., Pope, A., Halberstadt, A. R., Trusel, L., Cioffi, L., and Abdalati, W.: Antarctic Supraglacial Lake Detection Using Landsat 8 and Sentinel-2 Imagery: Towards Continental Generation of Lake Volumes, Remote Sensing, 12, 134, https://doi.org/10.3390/rs12010134, 2020.

Moussavi, M. S., Abdalati, W., Pope, A., Scambos, T., Tedesco, M., MacFerrin, M., and Grigsby, S.: Derivation and validation of supraglacial lake volumes on the Greenland Ice Sheet from high-resolution satellite imagery, Remote Sensing of Environment, 183, 294–303, https://doi.org/10.1016/j.rse.2016.05.024, <GotoISI>://WOS:000382345400024, type: Journal Article, 2016.

https://doi.org/10.5194/essd-2021-257
Preprint. Discussion started: 23 August 2021

Nunes, Vasco: fetchLandsatSentinelFromGoogleCloud: Python package to find and download Landsat and Sentinel-2 data from public storage on Google Cloud., https://github.com/vascobnunes/fetchLandsatSentinelFromGoogleCloud, since 2016.

Polsby, D. D. and Popper, R.: The Third Criterion: Compactness as a Procedural Safeguard Against Partisan Gerrymandering, SSRN Scholarly Paper ID 2936284, Social Science Research Network, Rochester, NY, https://doi.org/10.2139/ssrn.2936284, https://papers.ssrn.com/abstract=2936284, 1991.

Pope, A., Scambos, T. A., Moussavi, M., Tedesco, M., Willis, M., Shean, D., and Grigsby, S.: Estimating supraglacial lake depth in West Greenland using Landsat 8 and comparison with other multispectral methods, Cryosphere, 10, 15–27, https://doi.org/10.5194/tc-10-15-2016, <GotoISI>://WOS:000377602600002, type: Journal Article, 2016.

Rahmani, S., Strait, M., Merkurjev, D., Moeller, M., and Wittman, T.: An Adaptive IHS Pan-Sharpening Method, IEEE Geoscience and Remote Sensing Letters, 7, 746–750, https://doi.org/10.1109/LGRS.2010.2046715, conference Name: IEEE Geoscience and Remote Sensing Letters, 2010.

Reock, E. C.: A Note: Measuring Compactness as a Requirement of Legislative Apportionment, Midwest Journal of Political Science, 5, 70–74, https://doi.org/10.2307/2109043, https://www.jstor.org/stable/2109043, publisher: [Wiley, Midwest Political Science Association], 1961.

Rignot, E. and Irvine, U. O. C.: MEaSUREs InSAR-Based Antarctica Ice Velocity Map, Version 2, https://doi.org/10.5067/D7GK8F5J8M8R, https://nsidc.org/data/nsidc-0484/versions/2, type: dataset, 2017.

Rignot, E., Casassa, G., Gogineni, P., Krabill, W., Rivera, A., and Thomas, R.: Accelerated ice discharge from the Antarctic Peninsula following the collapse of Larsen B ice shelf, Geophysical Research Letters, 31, https://doi.org/10.1029/2004gl020697, <GotoISI>://WOS:000224125900003, type: Journal Article, 2004.

Rignot, E., Mouginot, J., and Scheuchl, B.: Ice Flow of the Antarctic Ice Sheet, Science, 333, 1427–1430, https://doi.org/10.1126/science.1208336, https://www.sciencemag.org/lookup/doi/10.1126/science.1208336, 2011.

Rignot, E., Jacobs, S., Mouginot, J., and Scheuchl, B.: Ice-shelf melting around Antarctica., Science (New York, N.Y.), 341, 266–270, https://doi.org/10.1126/science.1235798, https://escholarship.org/uc/item/0jm230gv, 2013.

Roberts, S. J., Hodgson, D. A., Bentley, M. J., Smith, J. A., Millar, I. L., Olive, V., and Sugden, D. E.: The Holocene history of George VI Ice Shelf, Antarctic Peninsula from clast-provenance analysis of epishelf lake sediments, Palaeogeography, Palaeoclimatology, Palaeoecology, 259, 258–283, https://doi.org/10.1016/j.palaeo.2007.10.010, https://www.sciencedirect.com/science/article/pii/S0031018207005147, 2008.

Scambos, T., Hulbe, C., and Fahnestock, M.: Climate-induced ice shelf disintegration in the Antarctic Peninsula, in: Antarctic Peninsula Climate Variability: Historical and Paleoenvironmental Perspectives, edited by Domack, E., Leventer, A., Burnett, A., Bindshadler, R., Convey, P., and Kirby, M., vol. 79 of *Antarctic Research Series*, pp. 79–92, American Geophysical Union (AGU), https://doi.org/10.1029/AR079p0079, <GotoISI>://WOS:000224376000007, type: Journal Article, 2003.

Scambos, T., Fricker, H. A., Liu, C.-C., Bohlander, J., Fastook, J., Sargent, A., Massom, R., and Wu, A.-M.: Ice shelf disintegration by plate bending and hydro-fracture: Satellite observations and model results of the 2008 Wilkins ice shelf break-ups, Earth and Planetary Science Letters, 280, 51–60, https://doi.org/10.1016/j.epsl.2008.12.027, https://www.sciencedirect.com/science/article/pii/S0012821X08007887, 2009.

Scambos, T. A., Hulbe, C., Fahnestock, M., and Bohlander, J.: The link between climate warming and break-up of ice shelves in the Antarctic Peninsula, Journal of Glaciology, 46, 516–530, https://doi.org/10.3189/172756500781833043, <GotoISI>://WOS:000165920700018, type: Journal Article, 2000.

https://doi.org/10.5194/essd-2021-257
Preprint. Discussion started: 23 August 2021

Siegert, M., Atkinson, A., Banwell, A., Brandon, M., Convey, P., Davies, B., Downie, R., Edwards, T., Hubbard, B., Marshall, G., Rogelj, J., Rumble, J., Stroeve, J., and Vaughan, D.: The Antarctic Peninsula Under a 1.5Â°C Global Warming Scenario, Frontiers in Environmental Science, 0, https://doi.org/10.3389/fenvs.2019.00102, https://www.frontiersin.org/articles/10.3389/fenvs.2019.00102/full, publisher: Frontiers, 2019.

Sneed, W. A. and Hamilton, G. S.: Evolution of melt pond volume on the surface of the Greenland Ice Sheet, Geophysical Research Letters, 34, https://doi.org/10.1029/2006gl028697, <GotoISI>://WOS:000244360500002, type: Journal Article, 2007.

Stokes, C. R., Sanderson, J. E., Miles, B. W. J., Jamieson, S. S. R., and Leeson, A. A.: Widespread distribution of supraglacial lakes around the margin of the East Antarctic Ice Sheet, Scientific Reports, 9, https://doi.org/10.1038/s41598-019-50343-5, <GotoISI>://WOS:000487586600014, type: Journal Article, 2019.

Tedesco, M., Luthje, M., Steffen, K., Steiner, N., Fettweis, X., Willis, I., Bayou, N., and Banwell, A.: Measurement and modeling of ablation of the bottom of supraglacial lakes in western Greenland, Geophysical Research Letters, 39, https://doi.org/10.1029/2011gl049882, <GotoISI>://WOS:000299393400001, type: Journal Article, 2012.

Tedesco, M., Willis, I. C., Hoffman, M. J., Banwell, A. F., Alexander, P., and Arnold, N. S.: Ice dynamic response to two modes of surface lake drainage on the Greenland ice sheet, Environmental Research Letters, 8, https://doi.org/10.1088/1748-9326/8/3/034007, <GotoISI>://WOS:000325247100013, type: Journal Article, 2013.

Trusel, L. D., Frey, K. E., Das, S. B., Karnauskas, K. B., Munneke, P. K., van Meijgaard, E., and van den Broeke, M. R.: Divergent trajectories of Antarctic surface melt under two twenty-first-century climate scenarios, Nature Geoscience, 8, 927–U56, https://doi.org/10.1038/ngeo2563, <GotoISI>://WOS:000367200200014, type: Journal Article, 2015.

Tuckett, P. A., Ely, J. C., Sole, A. J., Livingstone, S. J., Davison, B. J., Melchior van Wessem, J., and Howard, J.: Rapid accelerations of Antarctic Peninsula outlet glaciers driven by surface melt, Nature Communications, 10, 4311, https://doi.org/10.1038/s41467-019-12039-2, https://doi.org/10.1038/s41467-019-12039-2, type: Journal Article, 2019.

van der Veen, C. J.: Fracture propagation as means of rapidly transferring surface meltwater to the base of glaciers, Geophysical Research Letters, 34, https://doi.org/10.1029/2006gl028385, https://agupubs.onlinelibrary.wiley.com/doi/abs/10.1029/2006GL028385, type: Journal Article, 2007.

Williamson, A. G., Arnold, N. S., Banwell, A. F., and Willis, I. C.: A Fully Automated Supraglacial lake area and volume Tracking("FAST") algorithm: Development and application using MODIS imagery of West Greenland, Remote Sensing of Environment, 196, 113–133, https://doi.org/10.1016/j.rse.2017.04.032, <GotoISI>://WOS:000403443700009, type: Journal Article, 2017.

Williamson, A. G., Banwell, A. F., Willis, I. C., and Arnold, N. S.: Dual-satellite (Sentinel-2 and Landsat 8) remote sensing of supraglacial lakes in Greenland, Cryosphere, 12, 3045–3065, https://doi.org/10.5194/tc-12-3045-2018, <GotoISI>://WOS:000445625900002, type: Journal Article, 2018.

Xu, H.: Modification of normalised difference water index (NDWI) to enhance open water features in remotely sensed imagery, International Journal of Remote Sensing, 27, 3025–3033, https://doi.org/10.1080/01431160600589179, https://doi.org/10.1080/01431160600589179, type: Journal Article, 2006.

Yang, K. and Smith, L. C.: Supraglacial Streams on the Greenland Ice Sheet Delineated From Combined Spectral-Shape Information in High-Resolution Satellite Imagery, Ieee Geoscience and Remote Sensing Letters, 10, 801–805, https://doi.org/10.1109/lgrs.2012.2224316, <GotoISI>://WOS:000320720300009, type: Journal Article, 2013.